Supplementary Figure 1

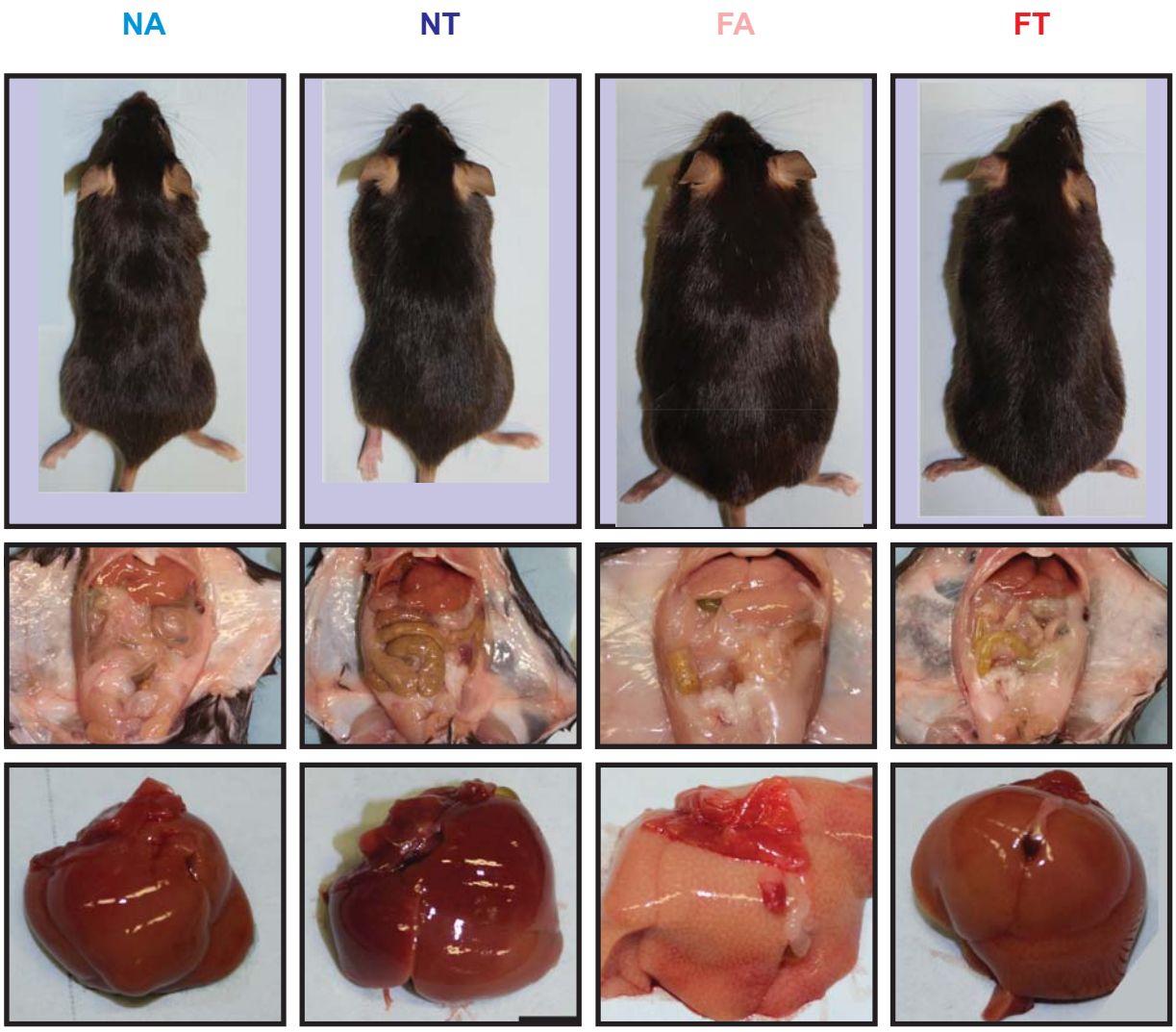

Supplementary Figure 2

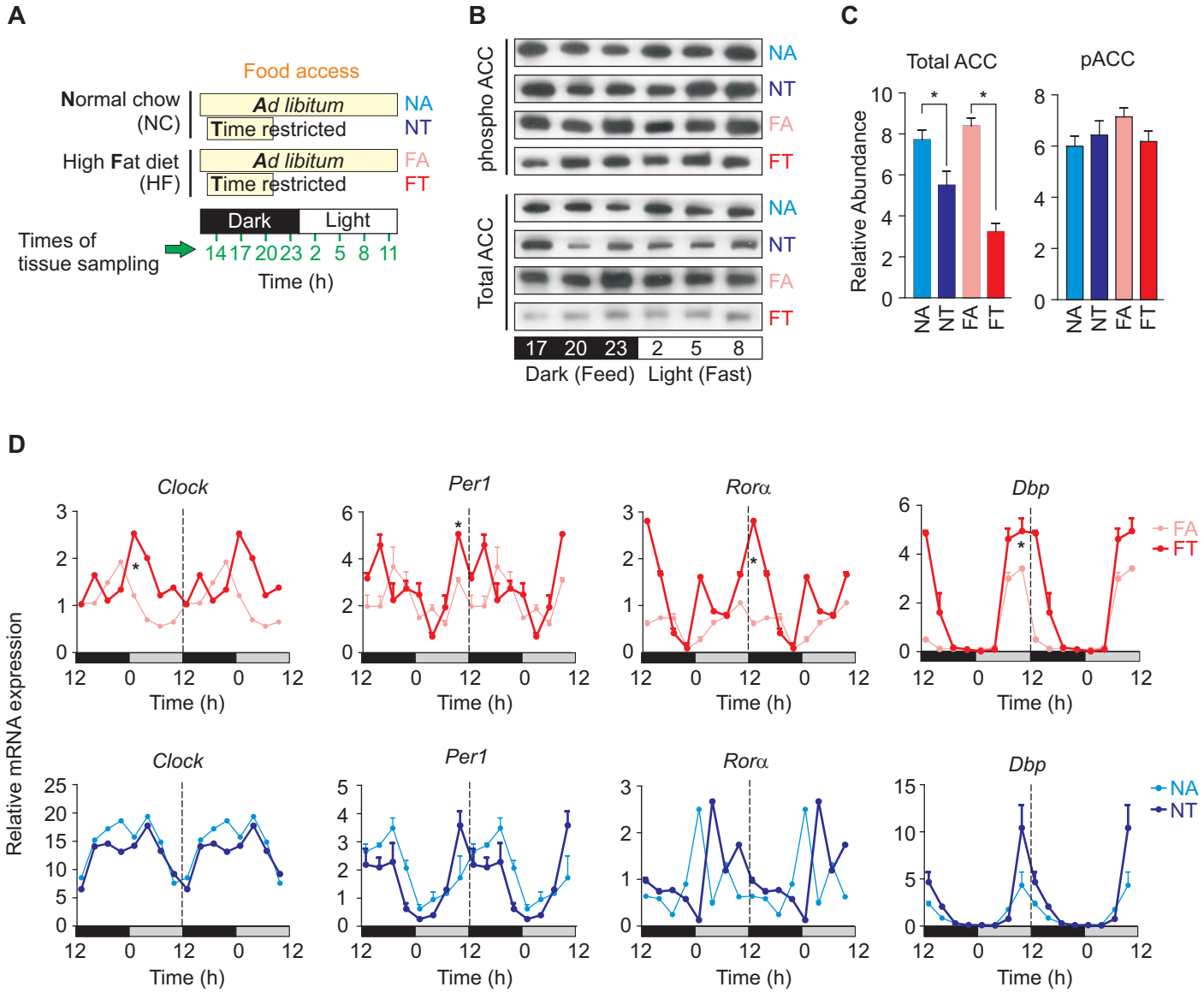

Supplementary Figure 3

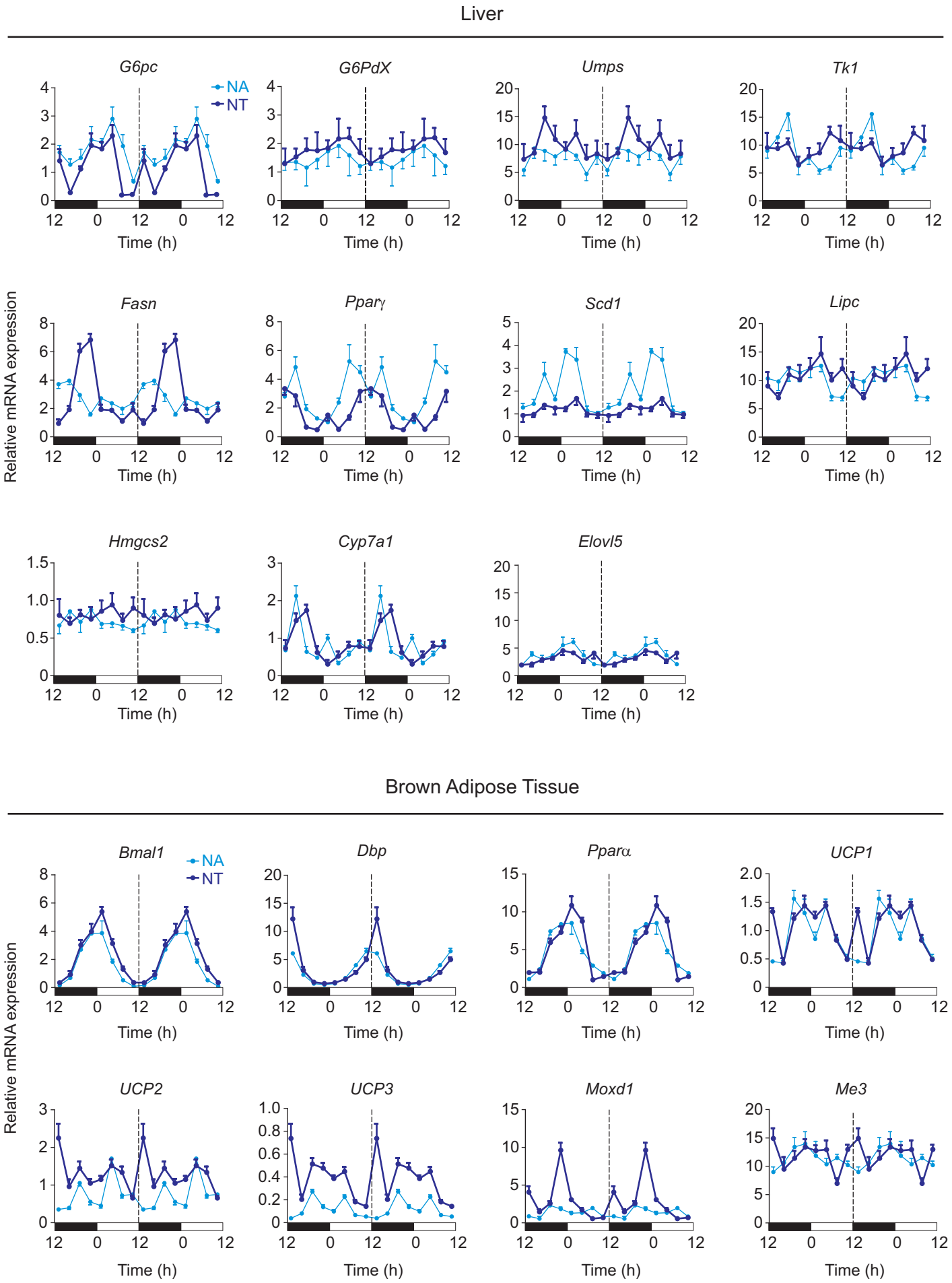

Supplementary Figure 4

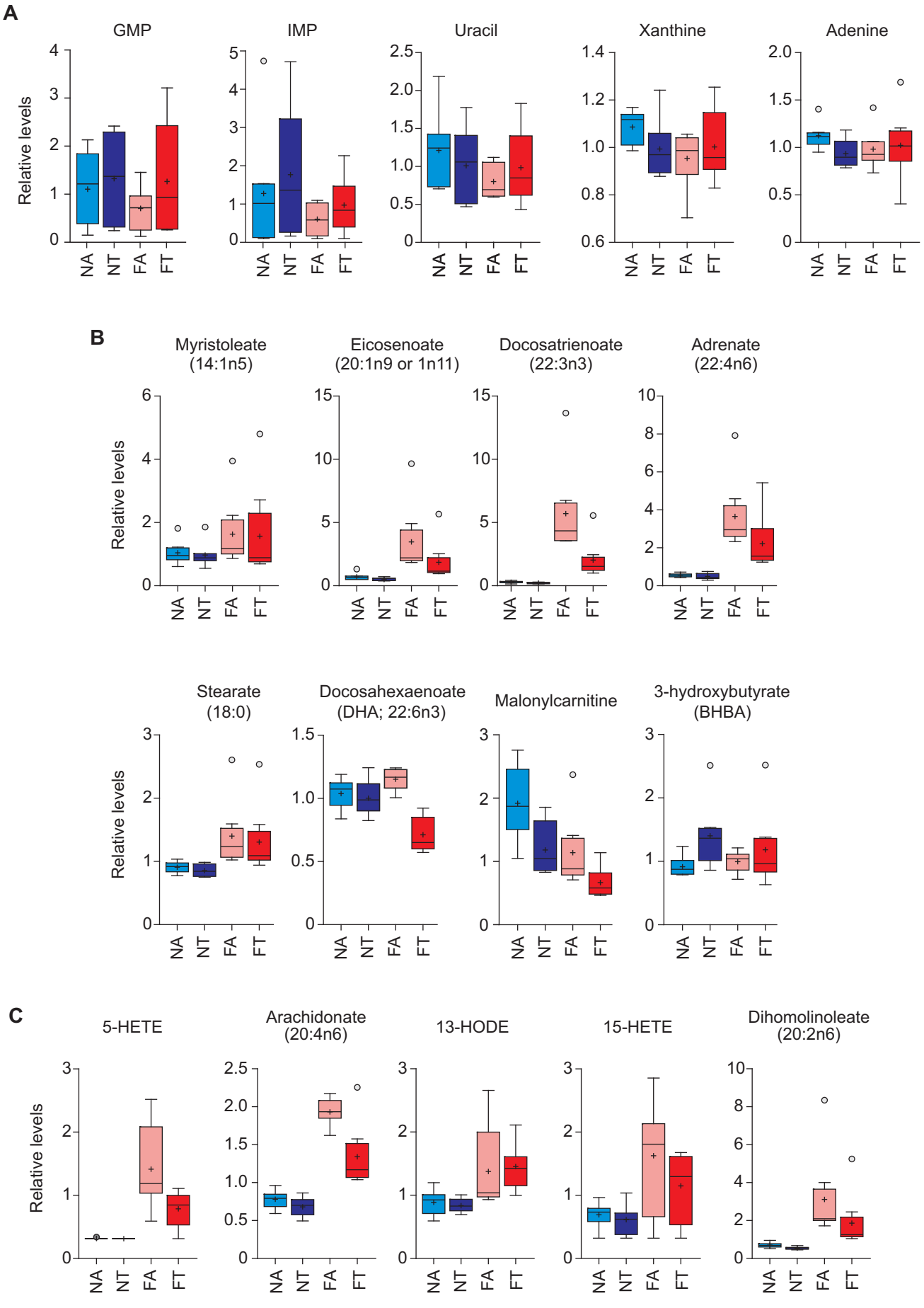

Supplementary Figure 5

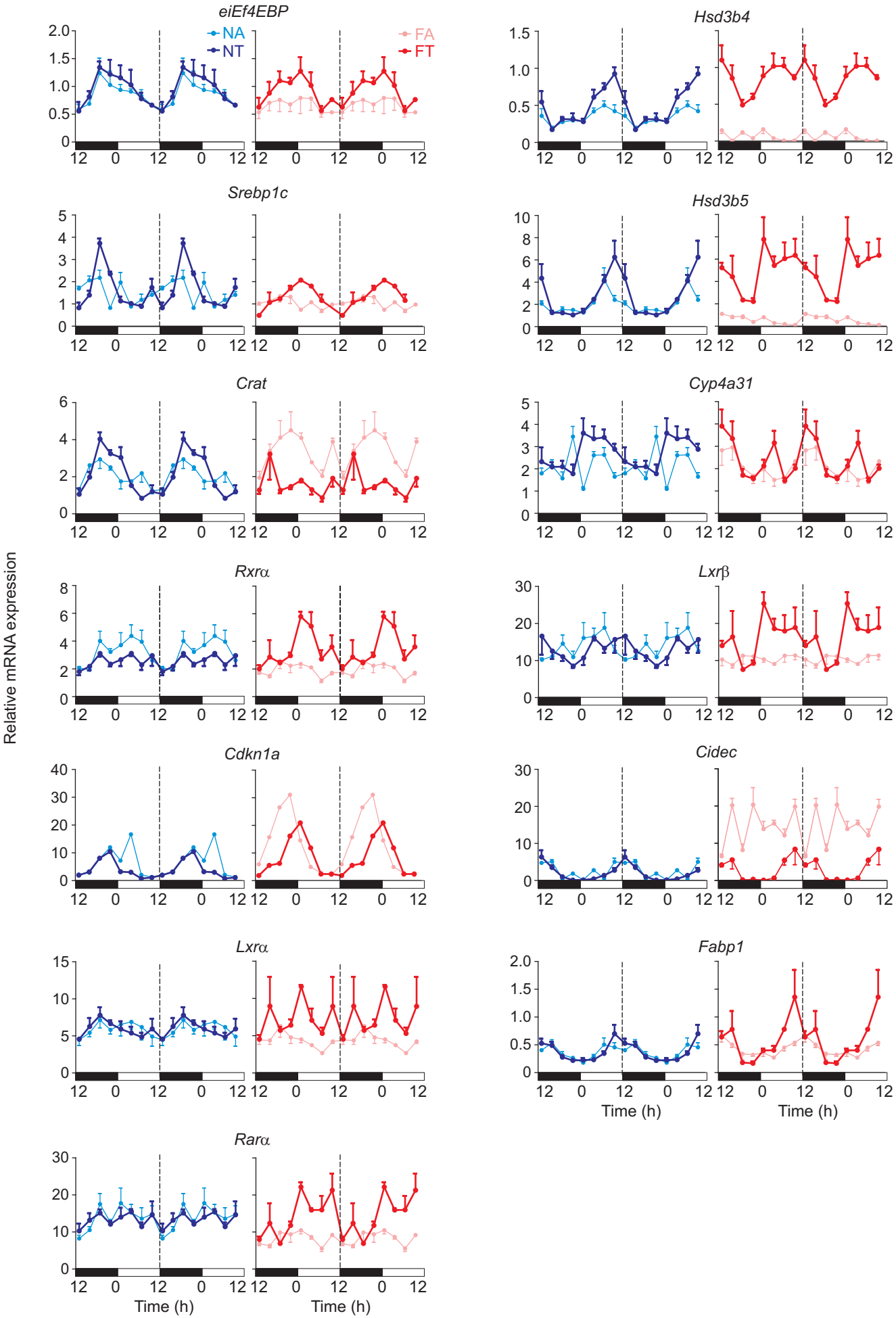

Supplementary Figure 5 (continued)

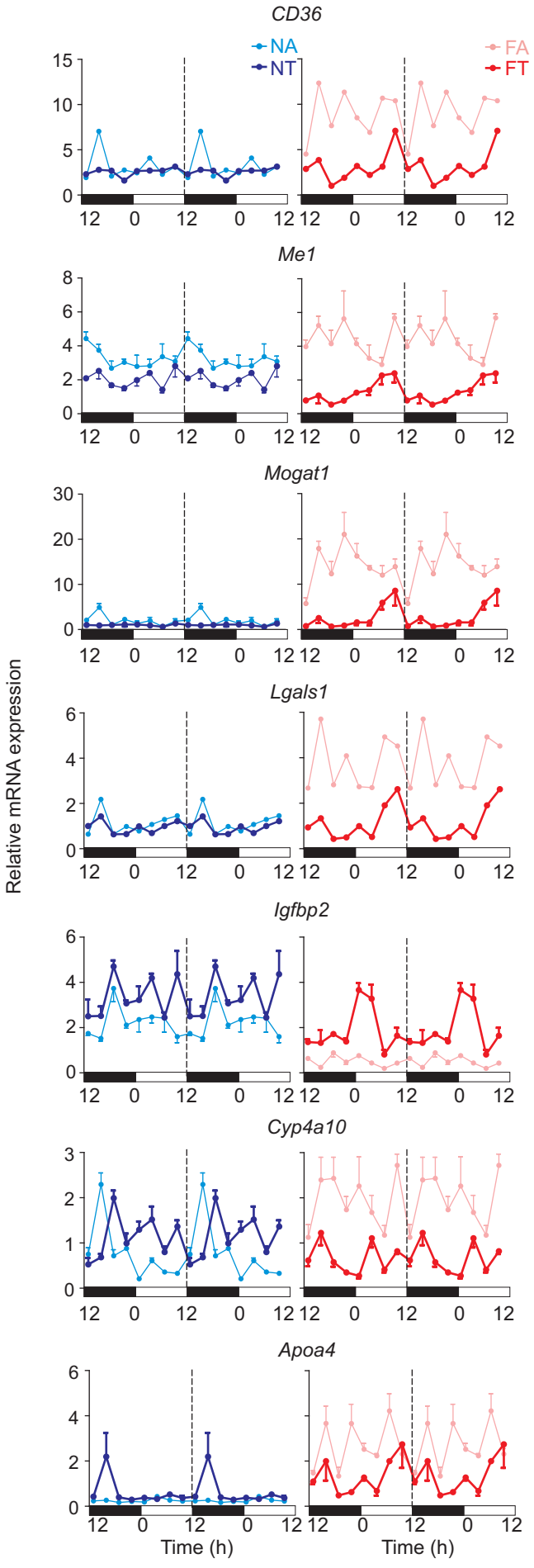

Supplementary Figure 6

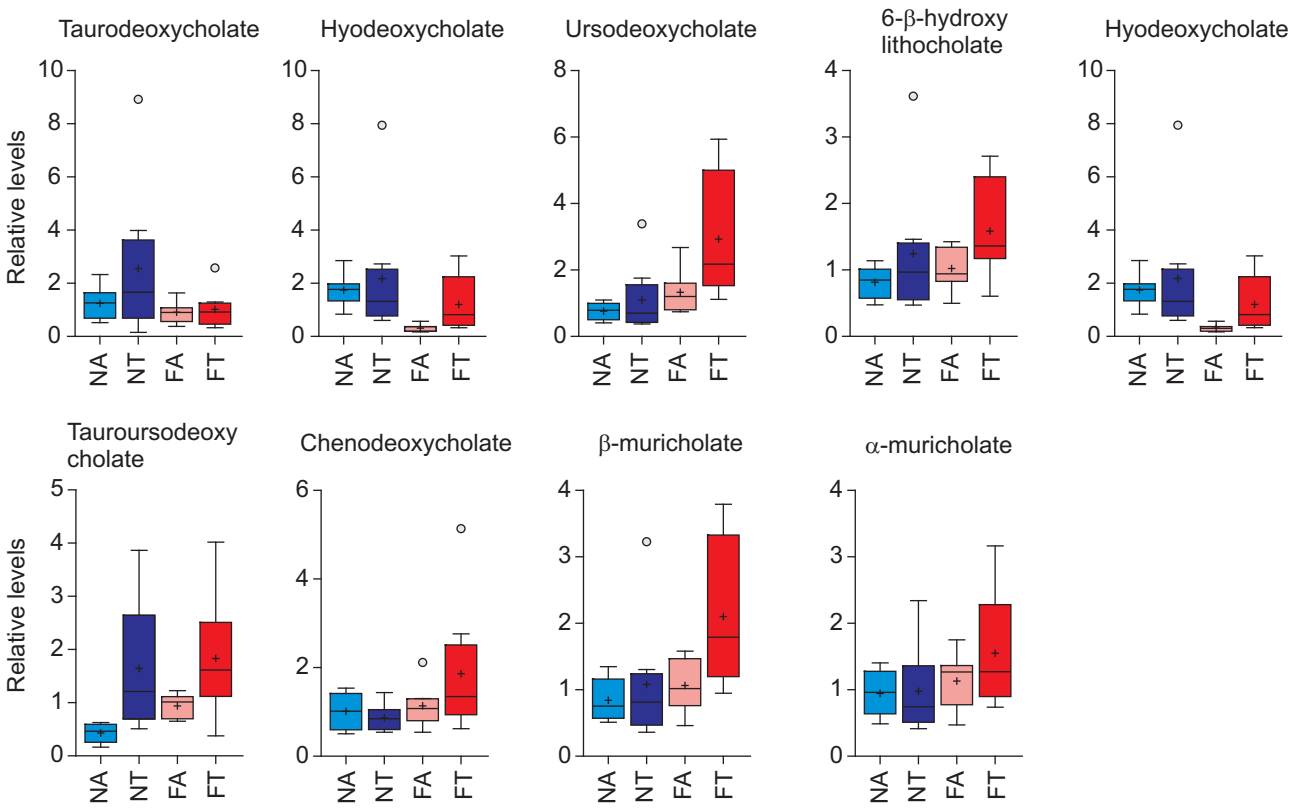

Supplementary Figure 7

Supplementary Information

Supplementary Figure and Table Legends

Supplementary Figure 1. Pictures of randomly selected whole body (top), body cavity (middle) and liver (bottom) of mice on NA, NT, FA and FT regimens. Mice were sacrificed after 18 weeks on different feeding regimen. Relates to Figure 1.

Supplementary Figure 2. Time restricted feeding restored normal activities of metabolic regulators and circadian rhythms in mice fed a high fat diet. (A) Schematic representation of time of tissue samples collected for RNA, protein and metabolite analyses. At each time point, 4 mice under each feeding regimen were sacrificed, and their tissues collected and flash frozen for subsequent analyses. Each frozen tissue sample was pulverized to a fine powder and split for RNA extraction, protein extraction and metabolite analyses. For immuno blot analyses shown in Figures 2A, 2B and S2B, liver samples from three time points corresponding to the time of food access in tRF mice and three time points that are 12 h away during the day time were analyzed. **(B)** Immuno blot analyses of phospho-ACC (pACC) and total ACC from the liver of four groups of mice during nighttime feeding or daytime fasting. Equal quantities of protein were loaded in each lane. No apparent diurnal change in ACC or pACC was detected. **(C)** Densitometric quantification of average (+ SEM, n = 6) levels of total ACC and pACC in the livers of four different groups of mice. The reduction in total ACC in the liver of mice under FT regimen is likely due to increased expression of its repressor REV-ERBα (Feng et al., 2011). **(D)** Double-plotted mean (+ SEM, n = 4) mRNA levels of *Clock*, *Per1*, *Rorα* and *Dbp* from the liver show improved oscillation under tRF paradigm. The levels of expression and/or the peak:trough ratios are remarkably increased in FT relative to FA liver, while the changes are modest between NA and NT groups.

Expression levels were measured by qRT-PCR and normalized against *Gapdh* mRNA. Results shown here relate to Figure 2.

Supplementary Figure 3. Temporal patterns of gene expression in mice fed a normal diet. Double-plotted average (+ SEM, n = 4) mRNA levels of genes regulating metabolism of glucose, nucleotides, fatty acids, cholesterol and bile acids in the liver or of circadian oscillator components, regulators of fat metabolism and mitochondria function in the BAT of NA and NT mice at different times of the day. Transcript levels were measured by qRT-PCR, and normalized to *Gapdh* RNA levels. Broken line separates double plotted data. Results relate to Figures 3, 4, and 6.

Supplementary Figure 4. Hepatic accumulation of nucleotide metabolites, free fatty acids and pro-inflammatory fatty acid metabolites are modulated under tRF paradigm. (A) Levels of several intermediates of nucleotide metabolism are increased in the liver of FT mice relative to their levels in FA mice. This is consistent with the changes in gene expression and in nucleotide metabolites shown in Figures 3F-3H. **(B)** Relative levels of representative long chain free fatty acids are increased in mice fed high fat diet. The levels of the majority of long chain free fatty acids detected were reduced in the liver of FT mice. Mice fed normal chow generally contained small amount of free fatty acids. Nevertheless, tRF paradigm further reduced the levels of hepatic free fatty acids. **(C)** Similar attenuation of pro-inflammatory fatty acids was observed in liver. Results presented in Figure S4B and S4C relate to Figure 4.

Supplementary Figure 5. Temporal hepatic gene expression pattern in mice fed a NC or HF diet under *ad lib* and tRF paradigms. Double-plotted average (+ SEM, n = 4) mRNA levels of genes implicated in protein translation, steroid metabolism and in several liver diseases are shown. Transcript

levels were measured by qRT-PCR, normalized to *Gapdh* RNA levels. Broken line separates double plotted data. Notice the overall changes in gene expression upon time restricted feeding is moderate in mice fed a normal diet, while temporal feeding pattern has a pronounced effect when mice are fed a high fat diet. Results relate to Figures 5 and 6.

Supplementary Figure 6. Bile acid levels are increased in the liver of FT mice compared to those found in the FA mice. Related to Figure 6

Supplementary Figure 7. **Relative levels and diurnal accumulation pattern of key liver metabolites in the mouse liver is defined by nutrient type and time of feeding.** Normalized levels of several metabolites at 8 different time points spaced at 3 h interval over one full day are shown for each of the four feeding groups (NA, NT, FA and FT). Times of measurement relative to light:dark cycle and periods of food access are shown at the bottom right panel. Values shown here relate to the whisker plots of metabolites shown in Figures 2-4, 6 and 7. Relative values and associated statistical parameters are shown in Table S1.

Supplementary Table 1. Liver metabolites and their relative abundance in mice fed normal chow or high fat diet under *ad lib* and tRF regimens. Biochemicals organized into super pathways, sub pathways, their method of detection, mass, reference CAS, Pubchem, KEGG and HMDB identifiers, raw data representing area under curve, scaled-, log transformed- and imputed- data, mean levels (n = 8 different time points), fold change, *p*-value and *q*-values are shown. Missing values for a given biochemical were replaced with minimum imputed values from the remainder of the samples. Percent filled values indicate the number of samples without imputed values. The dataset can also be accessed from a public website (http://metabolites.salk.edu). Relates to Figures 2-4, 6 and 7.

Supplementary Table 2. Major subcellular structures and their percent volume fraction in hepatocytes from FA and FT mice as determined by serial block face scanning electron microscopy of liver samples. Relates to Figure 5D.

Supplementary Data

Supplementary Table 2

	Percentage of volume	
	FT	FA
Mitochondrion	19.92%	8.24%
Cytosol	33.56%	24.19%
Vacuole	2.80%	16.05%
Nucleus	6.58%	2.60%
Capillaries	13.83%	8.57%
Glycogen	14.22%	5.75%
Lipid Body	0.58%	30.15%
Endoplasmic Reticulum	8.51%	4.45%

Supplementary Experimental Procedures

Histology and Electron Microscopy. Sections (6 μm) of formaldehyde fixed liver, WAT and BAT were stained following standard H&E. Liver sections were also stained using Sirius Red method. H&E and Steatohepatitis was scored using a semi-quantitative method derived from Brunt *et al*. (Brunt et al., 2004) measuring the degree of steatosis (0-3), ballooning degeneration (0-2), lobular (0-3) and portal (0-2) inflammation and fibrosis (0-4). Histology sections were digitally imaged using a fixed, high-resolution Leica DFC420 digital camera mounted on a Leica DMLS microscope. A serial block-face scanning electron microscopy (SBFSEM) volume was collected from both FT and FA liver following protocols as previously described (Williams et al., 2011), using a Gatan 3View system installed on a Zeiss Sigma SEM. Volumes were 12,000 pixel x 12,000 pixel x 500 slices with voxel dimensions of 5.63 nm XY x 70 nm Z. Image analysis was performed using IMOD (http://bio3d.colorado.edu/imod/). Stereology was performed using custom plug-in for IMOD.

Transcript, protein and metabolite analyses.

Anti-pACC, anti-ACC, anti-pS6 and anti-S6 antibodies were purchased from Cell Signaling Technologies (Cat No. 3661S, 3661S 4858S and 2217S, respectively). qRT-PCR primer sequence information is available upon request. For rhythmic transcripts, average expression (± SEM) from experimental replicates from each time point over 24 h are double plotted as line chart.

Supplementary References

Brunt, E.M., Neuschwander-Tetri, B.A., Oliver, D., Wehmeier, K.R., and Bacon, B.R. (2004). Nonalcoholic steatohepatitis: histologic features and clinical correlations with 30 blinded biopsy specimens. Human pathology 35, 1070-1082.

Feng, D., Liu, T., Sun, Z., Bugge, A., Mullican, S.E., Alenghat, T., Liu, X.S., and Lazar, M.A. (2011). A circadian rhythm orchestrated by histone deacetylase 3 controls hepatic lipid metabolism. Science 331, 1315-1319.

Williams, M.E., Wilke, S.A., Daggett, A., Davis, E., Otto, S., Ravi, D., Ripley, B., Bushong, E.A., Ellisman, M.H., Klein, G., and Ghosh, A. (2011). Cadherin-9 regulates synapse-specific differentiation in the developing hippocampus. Neuron 71, 640-655.